Plane-wave spectrum methods for the near-field characterization of very large structures using UAVs: The SKA radio telescope case

Quentin Gueuning*, Jean Cavillot†, Stuart Gregson‡, Christophe Craeye†
Eloy de Lera Acedo*, Anthony K Brown*‡, Clive Parini‡

*Cavendish Astrophysics, University of Cambridge, Cambridge, UK, qdg20@cam.ac.uk
†Antenna group, Universite catolique de Louvain, Louvain la Neuve, Belgium, jean.cavillot@uclouvain.be
‡School of Electronic Engineering and Computer Science, Queen Mary University of London, London, UK, stuart.gregson@qmul.ac.uk

***Abstract*—The reconstruction of embedded element patterns is analyzed in physically and electrically large aperture arrays from near-field measurements taken with a source carried by a drone. This is a very challenging metrology problem, especially when the arrays are composed of wide-band wide field-of-view antenna elements in a highly coupled environment, as is the case for the SKA-low radio telescope stations. We study the use of both a direct near- to far-field transformation and a model-based approach to overcome the limitations imposed by this type of complex electromagnetic structures. Both methods are explained using a decomposition of the antenna voltages in terms of a spectrum of incoming plane waves. A numerical example with an irregular array of 16 log-periodic elements and a hemispherical path shows their abilities to capture the mutual coupling effects.**

***Index Terms*—mutual coupling, measurements, plane-wave spectrum, spectral domain**

I. Introduction

The electromagnetic characterization of physically large structures is a difficult metrological challenge due to the size limitations imposed by existing test chambers. With the upcoming and emerging IoT technologies the presence of electromagnetic transceivers is expected to become ubiquitous in our societies, and this will translate into a growing demand for electromagnetic characterization of this type of structures (e.g. trains, buildings, etc) covered by networks of transceivers. The problem becomes even harder when the structures are electrically large and direct far-field measurements are not an option.

A particular case of interest for the authors of this paper is the calibration of future broadband radio telescopes composed of large phased arrays accounting for the effects of mutual coupling. In the context of the low-frequency SKA telescope project [1], this requires the characterization of the embedded element patterns (EEP) of each of the 256 dual-polarized log-periodic elements in 512 stations ($131,072$ separate elements) from 50 to 350 MHz, i.e. in a $7:1$ frequency band. Each station uses an irregular array of elements so in principle every element stands in a different electromagnetic environment [2]. The expected outcome of accurate calibration is an increase in dynamic range and imaging fidelity. The main constraints imposed by these arrays on their characterization are:

- The actual physical size of the arrays (38 m in diameter) and the impact of their local environment on their performance (e.g. soil conditions) call for an in-situ characterization system.
- Given that the far-field distance from the 38 m large SKA-low stations at 350 MHz is approximately 3.5 km, the far-field parameters such as gain, pattern, etc., require either a very expensive complex flying system if direct far-field measurements were to be done or alternatively, near-field measurements need to be considered.
- The wide field of view of these array antennas (90 degrees cone centred at zenith) requires a system capable of covering a large measurement area above the array, imposing limitations on the number of measurement points that may be taken by for example a UAV measurement system with limited flying time.
- The wide frequency band covered by these systems calls for a wide-band measurement system.
- The high mutual coupling in these arrays means that spatial features at scales proportional to the full size of the array may be expected and therefore the measurement system needs to provide enough resolution.

Traditionally, the calibration of arrays dedicated to radio-astronomy uses self-calibration. Self-calibration, which uses astronomical sources, is constrained by the reduced spatial coverage available and by the strong variations of the sky source intensities [3]. The proposed alternative consists of using an artificial source, with known radiation properties, carried on a UAV flying above the stations [4-8]. In order to compute the desired far-field parameters from near-field measurements, a mathematical transformation from one surface to another is required. It is well-known that this transformation, of arbitrary but monochromatic waves, can be performed efficiently by expressing the fields as a linear combination of

an elementary wave solution to Maxwell's equations. Here, the scalar coefficients of these solutions are usually found by matching them to the fields on the surface over which they are known and then by inverting the resulting integral with the use of mode orthogonality. Solving this expansion for the fields over a sphere of infinite radius that is centred on the AUT yields the asymptotic far-field pattern. Those methods require measurement with a source emitting with a stable phase in two orthogonal, tangential, polarizations and are known to be sensitive to the errors arising in the knowledge of positions and orientation of the source probe. Another class of methods [8][9][10] uses a simulation-based model of the current distribution on an a priori known antenna array which is then modified to match the measured data. In principle, this can help to reduce the number of required samples and the measurement time or to improve the resilience of the reconstructed pattern to probe positioning errors. However, errors are introduced related to reliability of the simulations due to uncertainty on the precise antenna geometry. In this paper, we study two methods based on these two approaches, that is a direct near- to far-field transformation and a method using a priori simulation–based knowledge of the embedded element patterns [8]. Their mathematical formulation is presented and numerical simulations are used to validate the two approaches.

II. Spectral-domain formulation of the near-field measurement problem

It is well-known that, by virtue of Lorentz's reciprocity theorem, the voltage v_n appearing at the output port of a passive antenna n when illuminated by a plane wave of incoming direction $\hat{\mathbf{u}}_i$ and of polarization $\tilde{\mathbf{E}}_i$ can be expressed by virtually assuming the antenna n as active while all the other antennas of the array remain passively terminated. This reads as [11]

$$v_n = \frac{2\lambda}{j\eta}\ Z_{L,n}\ \mathbf{f}_{e,n}(k\hat{\mathbf{u}}_i)\cdot\tilde{\mathbf{E}}_i \tag{1}$$

where k is the wavenumber, λ is the wavelength, η is the free-space impedance, $Z_{L,n}$ is the input impedance of the amplifier connected to antenna n. In this equation, the unitless embedded element pattern (EEP) $\mathbf{f}_{e,n}$ has been obtained by feeding antenna n with a Thevenin equivalent of impedance $Z_{L,n}$ and of unit voltage source and by using the array center as a common phase reference for every EEPs [12]. This definition does not follow the IEEE standards [13] but leads to a compact expression (1), and fully includes the effects of mutual coupling.

Let us now consider the more practical case of a drone carrying a dual-polarized antenna located at $\mathbf{r}_s$ and hovering at a near-field distance $r_s = ||\mathbf{r}_s||$ above the array. The electric field $\mathbf{E}_{s,p}$ radiated by the source probe p and impinging on antenna n can be decomposed into an angular spectrum of propagating and evanescent plane waves [15],

$$\mathbf{E}_{s,p}(\mathbf{r}_n) = \frac{1}{4\pi^2}\iint_{-\infty}^{\infty}\tilde{\mathbf{E}}_{s,p}(-\mathbf{k})\ e^{-j\mathbf{k}\cdot(\mathbf{r}_s-\mathbf{r}_n)}\ \mathrm{d}k_x\mathrm{d}k_y \tag{2}$$

where $\mathbf{r}_n$ is the position of antenna n, the reference z-axis is pointing up towards the drone, $\mathbf{k} = k_x\hat{\mathbf{x}} + k_y\hat{\mathbf{y}} + k_z\hat{\mathbf{z}}$ is the wavevector with ${k_z}^2 = k^2 - k_x^2 - k_y^2$ and the plane-wave spectrum of the incident field $\tilde{\mathbf{E}}_{s,p}$ is related to the "complex" pattern $\mathbf{f}_{s,p}$ of the source probe p, expressed in Volts, by

$$\tilde{\mathbf{E}}_{s,p}(\mathbf{k}) = \frac{2\pi}{jk_z}\ \mathbf{f}_{s,p}(\mathbf{k}) \tag{3}$$

From there, the voltage v_{np} induced on antenna n by probe p can be expressed by summing up the voltage contributions resulting from each incident plane wave using an analytical continuation of the relation (1) in which $\tilde{\mathbf{E}}_i$ and $k\hat{\mathbf{u}}_i$ are replaced by $\tilde{\mathbf{E}}_{s,p}/(4\pi^2)$ and $\mathbf{k}$, respectively. This yields

$$v_{np}(\mathbf{r}_s) = \frac{1}{4\pi^2}\iint_{-\infty}^{\infty}\tilde{v}_{np}(\mathbf{k})\ e^{-j\mathbf{k}\cdot\mathbf{r}_s}\ \mathrm{d}k_x\mathrm{d}k_y \tag{4}$$

with the plane-wave spectrum of the voltage defined by

$$\tilde{v}_{np}(\mathbf{k}) = \frac{-4\pi\lambda}{\eta k_z}\ Z_{L,n}\ \mathbf{f}_{e,n}(\mathbf{k})\cdot\mathbf{f}_{s,p}(-\mathbf{k}) \tag{5}$$

where the phase term $e^{j\mathbf{k}\cdot\mathbf{r}_n}$ is implicitly included in $\mathbf{f}_{e,n}(\mathbf{k})$. Relations (4) and (5) are widely known in antenna theory, when re-expressed in terms of scattering parameters or fields, as the transmission integral [14][16][17]. When the drone is not flying in the reactive field region, it is reasonable to neglect the multiple scattering between the drone and the array and to approximate the patterns in (5) as the EEP and the pattern of the isolated drone.

III. Model-based approach

An approach, presented in [8], uses full-wave simulations of the surface current $\mathbf{j}_n$ induced on the whole array when antenna n is active and decomposes it into $\mathbf{j}_n = \sum c_n^m \mathbf{j}_n^m$ where c_n^m are unknown calibration coefficients weighting the known part $\mathbf{j}_n^m$ of the current $\mathbf{j}_n$ flowing on antenna m. Hence, the EEP n is modelled by

$$\mathbf{f}_{e,n}(\mathbf{k}) = \sum_{m=1}^{N_a}\ c_n^m\ \mathbf{f}_{e,n}^m(\mathbf{k})\ e^{j\mathbf{k}\cdot\mathbf{r}_m} \tag{6}$$

where N_a is the number of antenna and the simulated patterns $\mathbf{f}_{e,n}^m(\mathbf{k})$ of each current $\mathbf{j}_{e,n}^m$ have been computed here using the center $\mathbf{r}_m$ of antenna m as a phase reference. Substituting (6) into (4), (5) and swapping sum and integral leads to

$$v_{np}(\mathbf{r}_s) = \sum_{m=1}^{N_a} c_n^m v_{np}^m(\mathbf{r}_{sm}) \tag{7}$$

where $\mathbf{r}_{sm} = \mathbf{r}_s - \mathbf{r}_m$ is the vector linking the center of antenna m to the drone and the voltage v_{np}^m is obtained by replacing $\mathbf{f}_{e,n}(\mathbf{k})$ with $\mathbf{f}_{e,n}^m(\mathbf{k})$ in (5). Assuming that the far-field pattern $\mathbf{f}_{s,p}$ of the drone is known, the voltages v_{np}^m can be computed numerically. This allows us to stack the N_a unknown coefficients c_n^m into a vector $\mathbf{c}_n$ and the L measured voltages $v_{np}(\mathbf{r}_{s,l})$ into a vector $\mathbf{v}_n$ and rewrite (7) as a linear system of equations $\mathbf{A}_n\mathbf{c}_n = \mathbf{v}_n$, where $\mathbf{A}_n$ is a $L \times N_a$ matrix with its (l,m) entry given by $A_{lm} = v_{np}^m(\mathbf{r}_{sm,l})$. The

calibration coefficients $\mathbf{c}_n$ are then determined by inverting $\mathbf{A}_n$ using a least squares solver.

A compact approximation of the voltages v_{np}^m can be obtained using the stationary phase method [20],[21]. Indeed, using equation (8) of [22], the spectral integral (4) can be approximated as:

$$v_{np}^m(\mathbf{r}_s) \simeq \frac{j}{2\pi}\ \tilde{v}_{np}^m(k\hat{\mathbf{u}}_{sm})\ \frac{e^{-jkr_{sm}}}{r_{sm}}\ k\cos(\theta_{sm}) \qquad (8)$$

where $k\hat{\mathbf{u}}_{sm}$ corresponds to the stationary point, $\mathbf{u}_{sm}$ is the direction vector centered on the antenna and pointing to the probe with elevation angle θ_{sm} and $r_{sm} = ||\mathbf{r}_{sm}||$ is the distance between the drone and the antenna. After including (5) in (8), one can see that this result leads to the far-field approximation proposed in [8],

$$v_{np}^m(\mathbf{r}_{sm}) \simeq \frac{8\pi\lambda}{j\eta}\ Z_{L,n}\ G(k, r_{sm})\ \mathbf{f}_{e,n}(k\hat{\mathbf{u}}_{sm}) \cdot \mathbf{f}_{s,p}(-k\hat{\mathbf{u}}_{sm}) \qquad (9)$$

where $G(k, r_{sm}) = e^{-jkr_{sm}}/(4\pi r_{sm})$ is the three-dimensional free-space Green's function. The error induced by the asymptotic approximation (9) on the reconstructed EEP will be illustrated in Section V.

IV. Near- to far-field transformation

Typically, the transmission equation (4) is inverted by exploiting mode orthogonality and it is convenient to express the surface profile on which the near-field is defined as a function of two coordinates, x and y, where the coordinates are plaid, monotonic and equally spaced. For a smooth surface, such as a hemisphere, defined by a function $g(x, y, z)$ we can thus define the element of area da and inwardly facing unit normal which varies over the surface of integration [19]. So taking the "measured" drone data over a sphere we first interpolate the field points onto a regular plaid, monotonic and equally spaced spherical grid, add a Cosine^2 window function and transform the data to the far-field. Here we have used a window function beginning at 60° in elevation out to 90° (horizontal) to avoid the sudden field truncation that occurs without window for this electrically small element with strong field values in the horizontal plane. It is important to note that within this derivation we have assumed that all measurements were performed with the same probe in the same orientation whereby standard probe compensation may be utilised, or with an infinitesimal Hertzian dipole probe upon probe correction, may be dispensed with altogether. If this is not the case, then the probe influence should be included within the forward equation (4) so that its influence is directly considered within the equation system inversion.

V. Numerical results

We analyze here the reconstruction of one EEP at 175 MHz, i.e. wavelength $\lambda = 1.7$ m, of an irregular array of 16 SKA Log-periodic Antennas (SKALA2 [23],see Fig. 1) lying on top of an infinite ground plane, as depicted in Fig. 2. The antenna under consideration lies close to the array center. As sketched in Fig. 2, the drone starts from the top of an hemisphere of 15 m radius, i.e. roughly 9λ, then follows rings of constant elevation and gradually goes down until it reaches the ground. With this trajectory, the hemisphere is sampled uniformly in elevation and azimuth every 2° and the drone stands well in the array near-field since the far-field distance is 75 m at 175 MHz. It is also important to note that the drone hovers at an intermediate-field distance of every antenna since their far-field distance, including the antenna image, is 20 m.

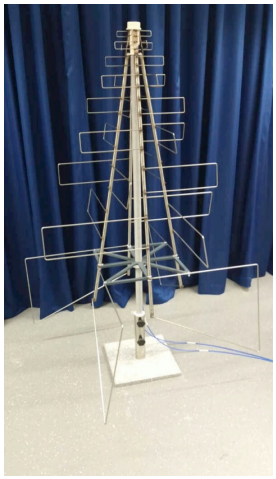

Fig. 1. Second version of the SKA Log-periodic Antenna (SKALA2) [23]

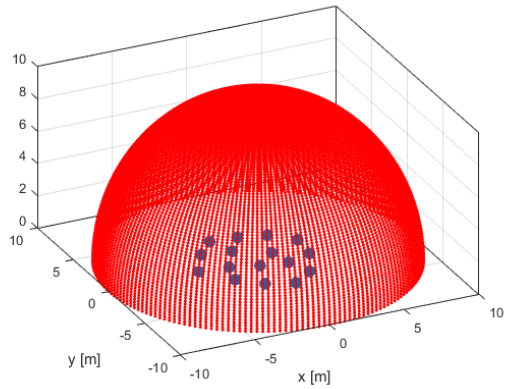

Fig. 2. Array layout and example of the near-field sampling path

The components of the isolated element pattern and the actual EEP are depicted alongside in Fig 3. One can observe ripples of around 5 dB in the EEP caused by the mutual coupling between antennas. In the following figures, we will show the absolute error on the reconstructed EEP obtained as follows:

$$\epsilon(dB) = 20\log_{10}|E - \hat{E}| \qquad (10)$$

where E and $\hat{E}$ are, respectively, the x-y component of the exact far field and the field reconstructed using either the near- to far-field transformation or the model-based approach.

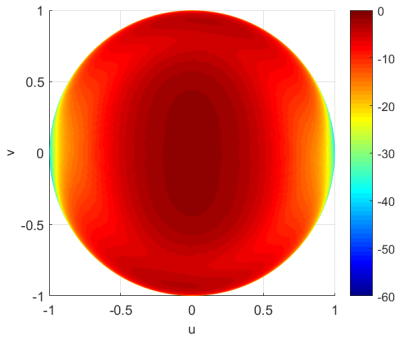

(a)

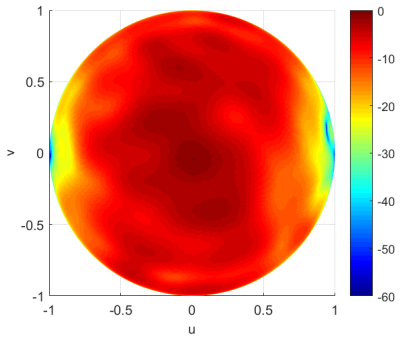

(b)

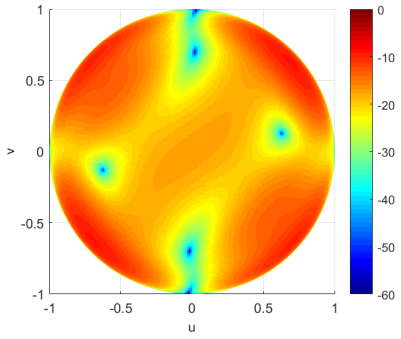

(c)

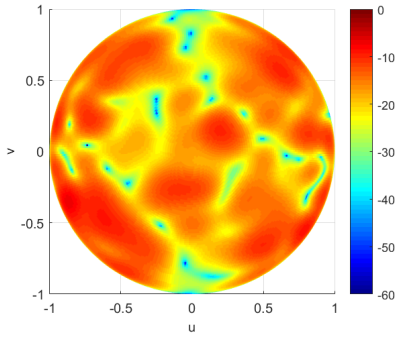

(d)

Fig. 3. (a) x-component of the isolated element pattern, (b) x-component of the EEP, (c) y-component of the isolated element pattern, (d) y-component of the EEP.

Fig. 4 shows the error in the reconstructed far-field pattern using the model-based approach of Section III. The error level is around -20 dB at zenith, this may come from the far field approximation done in (9) since, as mentioned previously, the drone stands also in the near field of every antenna. Fig. 5 shows the corresponding reconstruction error based on the near- to far-field transformation described in Section IV. In this case the peak error in the 90° cone about zenith is -45 dB with around -55 dB in the central region. The level of agreement is demonstrated by comparing the contour plots for both the simulated and transformed EEPs in Fig. 6.

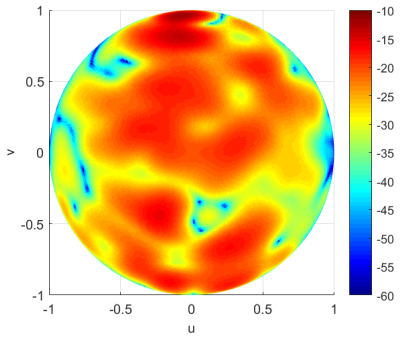

(a)

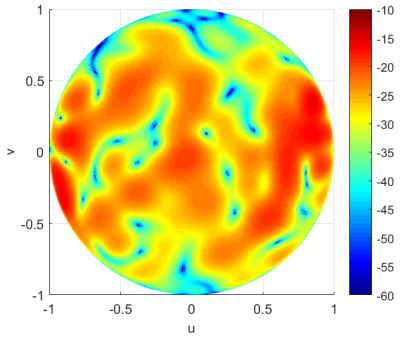

(b)

Fig. 4. x- (a) and y- (b) components of the error, model-based approach

VI. Conclusion

Two plane wave spectrum methods for the electromagnetic characterisation of physically and electrically large structures have been analyzed with results shown for a specific radio astronomy application. The transformation approach offers an accurate solution but requires that the amplitude and phase of the signal from the drone be measured. A continuation of this work will study the impact of sub-Nyquist sampling and drone positional errors (eg. use of irregular measurement grids) on the performance of both methods.

The team is also now preparing for the further development of the methods and a measurement campaign with a 64-element array of SKALA4 antennas at the Mullard Radio Astronomy Observatory in Cambridge, UK.

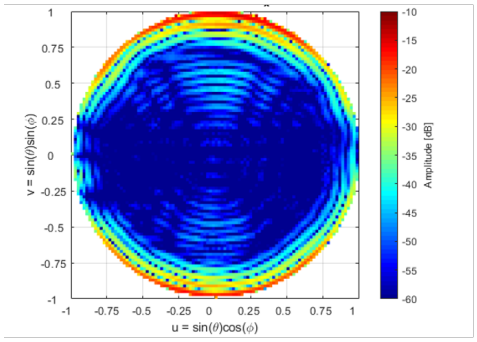

(a)

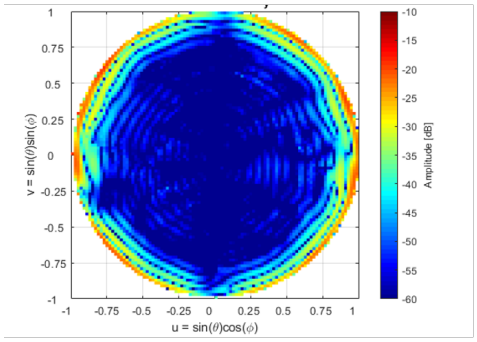

(b)

Fig. 5. x- (a) and y- (b) component of the error, transformation approach

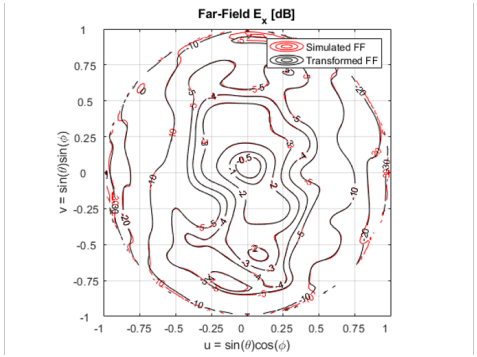

(a)

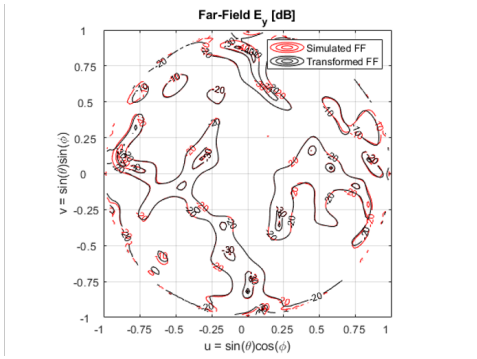

(b)

Fig. 6. Contour plot of the x- (a) and y- (b) components of the error, transformation approach

REFERENCES

[1] www.skatelescope.org

[2] E. de Lera Acedo, et al., "SKA LFAA Station Design Report", arXiv:2003.12744 [cs], Mar 2018.

[3] C. Lonsdale, "Calibration approaches," MIT Haystack, Tech. Rep. LFD memo 015, Dec. 2004.

[4] Fritzel, T., Strauß, R., Steiner, H., Eisner, C., and Eibert, T. F., "Introduction into an UAV-based near-field system for in-situ and large-scale antenna measurements (invited paper)," *in: Proc. IEEE Conference on Antenna Measurements Applications (CAMA)*, 2016.

[5] M. Garcia-Fernandez et al., "Antenna Diagnostics and Characterization Using Unmanned Aerial Vehicles," *in IEEE Access*, vol. 5, pp. 23563-23575, 2017.

[6] G. Virone, A. M. Lingua, M. Piras, A. Cina, F. Perini, J. Monari, F. Paonessa, O. A. Peverini, G. Addamo, and R. Tascone, "Antenna pattern verification system based on a micro unmanned aerial vehicle (UAV)," *IEEE Antennas and Wireless Propagation Letters*, vol. 13, pp. 169–172, 2014.

[7] P. Bolli, G. Pupillo, F. Paonessa, G. Virone, S. J. Wijnholds and A. M. Lingua, "Near-Field Experimental Verification of the EM Models for the LOFAR Radio Telescope," *IEEE Antennas and Wireless Propagation Letters*, vol. 17, no. 4, pp. 613-616, April 2018, doi: 10.1109/LAWP.2018.2805999.

[8] L. V. Hoorebeeck, J. Cavillot, H. Bui-Van, F. Glineur, C. Craeye and E. de Lera Acedo, "Near-field calibration of SKA-Low stations using unmanned aerial vehicles," *13th European Conference on Antennas and Propagation (EuCAP)*, Krakow, Poland, 2019, pp. 1-5.

[9] G. Giordanengo, M. Righero, F. Vipiana, G. Vecchi and M. Sabbadini, "Fast Antenna Testing With Reduced Near Field Sampling," *IEEE Transactions on Antennas and Propagation*, vol. 62, no. 5, pp. 2501-2513, May 2014.

[10] M. A. Saporetti et al., "Reduced Sampling in NF Antenna Measurement Using Numerical Defined Expansion Functions," *13th European Conference on Antennas and Propagation (EuCAP)*, Krakow, Poland, 2019, pp. 1-4.

[11] P.S. Kildal, *Foundations of Antenna Engineering: A Unified Approach for Line-of-Sight and Multipath*, Artech, 2015.

[12] C. Craeye and D. González-Ovejero, "A review on array mutual coupling analysis", *Radio Sci.*, vol. 46, no. 2, pp. 1-25, 2011.

[13] IEEE Standard for Definitions of Terms for Antennas - Redline," *in IEEE Std 145-2013 (Revision of IEEE Std 145-1993) - Redline* , pp.1-92, Mar. 2014.

[14] C.G. Parini, S.F. Gregson, J. McCormick, D. Janse Van Rensburg, *Theory and Practice of Modern Antenna Range Measurements*, IET Press, 2014.

[15] P. C. Clemmow, *The plane wave spectrum representation of electromagnetic fields*, Pergamon, 1966.

[16] D. M. Kerns, Plane- Wave Scattering-Matrix Theory of Antennas and Antenna-Antenna Interactions. Nat. Bur. Stand. Monograph 162, June 1981.

[17] A. D. Yaghjian, "Efficient computation of antenna coupling and fields within the near-field region," *IEEE Trans. Antennas Propag.*, vol. 30, no. 1, pp. 113–128, Jan. 1982.

[18] J. P. Hamaker, J. D. Bregman and R. J. Sault, "Understanding radio polarimetry: I. Mathematical foundations", *Astron. Astrophys. Suppl.*, vol. 117, 1996.

[19] S. Gregson, J. McCormick and C. Parini, *Principles of Planar Near-Field Antenna Measurements*, IET press 2007.

[20] N. Chako, "Asymptotic expansions of double and multiple integrals occuring in diffraction theory," *IMA J. Appl. Math.* , vol. 1, pp. 372–422, 1965.

[21] L. B. Felsen and N. Marcuvitz, *Radiation and Scattering of Waves.* Englewood Cliffs, NJ: Prentice-Hall, 1973.

[22] O. M. Conde, J. Perez and M. P. Catedra, "Stationary phase method application for the analysis of radiation of complex 3-D conducting structures," *in IEEE Transactions on Antennas and Propagation*, vol. 49, no. 5, pp. 724-731, May 2001, doi: 10.1109/8.929626

[23] E. de Lera Acedo, N. Razavi-Ghods, N. Troop, N. Drought, and, A. J. Faulkner, "SKALA, a log-periodic array antenna for the SKA-low instrument: design, simulations, tests and system considerations," *Exp. Astron.*, vol. 39, no. 3, pp. 567-594, Jul. 2015.